This is a repository copy of *Use of the time constant related parameter fmax to calculate the activation energy of bulk conduction in ferroelectrics*.

White Rose Research Online URL for this paper:
http://eprints.whiterose.ac.uk/134547/

Version: Accepted Version

Article:
Yang, F., Li, L., Wu, P. et al. (3 more authors) (2018) Use of the time constant related parameter fmax to calculate the activation energy of bulk conduction in ferroelectrics. Journal of Materials Chemistry C, 6 (34). pp. 9258-9268. ISSN 2050-7526

https://doi.org/10.1039/C8TC03011A

Reuse
Items deposited in White Rose Research Online are protected by copyright, with all rights reserved unless indicated otherwise. They may be downloaded and/or printed for private study, or other acts as permitted by national copyright laws. The publisher or other rights holders may allow further reproduction and re-use of the full text version. This is indicated by the licence information on the White Rose Research Online record for the item.

Takedown
If you consider content in White Rose Research Online to be in breach of UK law, please notify us by emailing eprints@whiterose.ac.uk including the URL of the record and the reason for the withdrawal request.

eprints@whiterose.ac.uk
https://eprints.whiterose.ac.uk/

Check for updates

View Article Online
View Journal

Journal of
Materials Chemistry C

Accepted Manuscript

This article can be cited before page numbers have been issued, to do this please use: F. Yang, L. Li, P. Wu, E. Pradal-Velázquez, H. K. Pearce and D. Sinclair, *J. Mater. Chem. C*, 2018, DOI: 10.1039/C8TC03011A.

This is an Accepted Manuscript, which has been through the Royal Society of Chemistry peer review process and has been accepted for publication.

Accepted Manuscripts are published online shortly after acceptance, before technical editing, formatting and proof reading. Using this free service, authors can make their results available to the community, in citable form, before we publish the edited article. We will replace this Accepted Manuscript with the edited and formatted Advance Article as soon as it is available.

You can find more information about Accepted Manuscripts in the author guidelines.

Please note that technical editing may introduce minor changes to the text and/or graphics, which may alter content. The journal's standard Terms & Conditions and the ethical guidelines, outlined in our author and reviewer resource centre, still apply. In no event shall the Royal Society of Chemistry be held responsible for any errors or omissions in this Accepted Manuscript or any consequences arising from the use of any information it contains.

ROYAL SOCIETY OF CHEMISTRY

rsc.li/materials-c

View Article Online
DOI: 10.1039/C8TC03011A

Journal Name

ARTICLE

Use of the time constant related parameter f_{max} to calculate the activation energy of bulk conduction in ferroelectrics

F. Yang,* L. Li, P. Wu, E. Pradal-Velázquez, H. K. Pearce and D. C. Sinclair*

Received 00th January 20xx,
Accepted 00th January 20xx

DOI: 10.1039/x0xx00000x

www.rsc.org/

The activation energy associated with bulk electrical conduction in functional materials is an important quantity which is often determined by impedance spectroscopy using an Arrhenius-type equation. This is achieved by linear fitting of bulk conductivity obtained from complex (Z*) impedance plots versus T^{-1} which gives an activation energy $E_a(\sigma)$ or by linear fitting of the characteristic frequency f_{max} obtained from the large Debye peak in M''-log$f$ spectroscopic plots against T^{-1} which gives an activation energy $E_a(f_{max})$. We report an analysis of $E_a(\sigma)$ and $E_a(f_{max})$ values for some typical non-ferroelectric and ferroelectric materials and employ numerical simulations to investigate combinations of different conductivity-temperature and permittivity-temperature profiles on the logf_{max} – T^{-1} relationship and $E_a(f_{max})$. Results show the logf_{max} – T^{-1} relationship and $E_a(f_{max})$ are strongly dependent on the permittivity-temperature profile and the temperature range measured relative to T_m (temperature of the permittivity maximum). Ferroelectric materials with a sharp permittivity peak can result in non-linear logf_{max} – T^{-1} plots in the vicinity of T_m. In cases where data are obtained either well above or below T_m, linear logf_{max} – T^{-1} plots can be obtained but overestimate or underestimate the activation energy for conduction, respectively. It is therefore not recommended to use $E_a(f_{max})$ to obtain the activation energy for bulk conduction in ferroelectric materials, instead $E_a(\sigma)$ should be used.

Introduction

Ferroelectrics are an important class of functional materials. They exhibit spontaneous polarisation below the ferroelectric Curie temperature (T_c) and have a wide range of applications in capacitors, sensors, actuators and optical or memory devices. [1, 2] Electrical conductivity and the conduction mechanism(s) in ferroelectric materials are critical to their properties, e.g., dielectric loss (tan δ), leakage current and Polarisation-Electric field hysteresis loops. For example, recent Impedance Spectroscopy studies on the lead-free $Na_{0.5}Bi_{0.5}TiO_3$ (NBT) ferroelectric perovskite reveal dramatic changes in the conduction mechanism with small changes in the A-site (Na,Bi) content. [3-6] Na-rich or Bi-deficient NBT compositions are oxide-ion conductors, exhibit high bulk conductivity (σ_b) with an activation energy (E_a) of 0.45 – 0.85 eV and display a sharp rise in tan δ with increasing temperature which exceeds 0.2 at ~ 623 K. In contrast, Bi-rich or Na-deficient NBT are electronically insulating with low bulk conductivity with E_a of ~ 1.7 eV and presents low tan δ over a wide temperature range (< 0.02 from 573 to 873 K) making them excellent dielectric materials. In-depth investigations of the bulk (grain) electrical conductivity and its associated activation energy can provide useful information to understand/predict the defect chemistry of a material and consequently on how to use chemical doping to improve/enhance the desired properties accordingly.

Department of Materials Science & Engineering, University of Sheffield, Mappin Street, Sheffield, S1 3JD, United Kingdom.
* Corresponding authors. fan.yang@sheffield.ac.uk; d.c.sinclair@sheffield.ac.uk

ac impedance spectroscopy is a powerful technique to study the electrical and dielectric properties of materials. Measurements are carried out over a wide range of frequency (typically milli- to mega-Hz) and different electro-active regions, e.g., bulk (grains), grain boundaries, surface layers, electrode effects, can be identified and characterised according to their electrical relaxation times or time constants.[7] As the various time constants usually differ by several orders of magnitude and they generally have different temperature dependencies (i.e., E_a values) it is necessary to make measurements over a wide temperature range to ensure comprehensive characterisation of the various electro-active regions.

Impedance data are conventionally plotted in the impedance spectrum (Z*) and fitted by an equivalent circuit which is some combination of resistors (R), Capacitors (C) and/or Constant Phase Elements (CPE). Typically, each electro-active region in a ceramic is modelled on a "parallel RC, R-CPE or R-C-CPE element" and these are often connected in series according to the Brick-layer model.[8] Each element gives rise to an arc in the Z* plot (providing its time constant is within the measured frequency range) and this can be used to obtain the R and C of each response. Resistance can be converted to conductivity and plotted as a function of reciprocal of temperature to obtain the activation energy, according to the Arrhenius equation

$$\sigma = \sigma_0 \exp\left[-\frac{E_a(\sigma)}{k_B T}\right], \quad (1)$$

where σ_0 is a pre-exponential factor, k_B is the Boltzmann constant and T is the absolute temperature. Impedance data can also be presented in complex electric modulus (M*), admittance (Y*) and permittivity (ε*) formalisms according to[9]

Published on 13 August 2018. Downloaded by University of Sheffield on 8/14/2018 9:16:36 AM.

Journal of Materials Chemistry C Accepted Manuscript

Please do not adjust margins

$$M^* = j\omega C_0 Z^* \quad (2a)$$

$$Y^* = \frac{1}{Z^*} \quad (2b)$$

$$\varepsilon^* = \frac{1}{M^*} \quad (2c)$$

where ω and C_0 in Eq.(2a) are the angular frequency and the capacitance of an empty cell, respectively; *j* is the square root of -1. Alternatively, spectroscopic plots of real and/or imaginary components of the various formalisms can be plotted to provide information that is not easily accessible from the complex impedance plane alone.[7] In particular, the M''- log*f* spectroscopic plot is useful to identify and characterise the bulk response in ceramics as it highlights the component with the smallest capacitance. The M''-log*f* plot usually displays a large Debye peak associated with the bulk response. The peak height is proportional to the reciprocal of capacitance and the frequency at which the M'' Debye peak reaches its maximum, f_{max}, is a characteristic relaxation frequency described by

$$2\pi f_{max} RC = 2\pi f_{max}\tau = 1, \quad (3)$$

where τ is the time constant. Studies on a variety of materials [10-16] show that f_{max} (or τ) can also obey the Arrhenius law and exhibit a linear relationship with T^{-1}, as described by

$$f_{max} = f_0 \exp\left[-\frac{E_a(f_{max})}{k_B T}\right], \quad (4)$$

where f_0 is the pre-exponential factor. In these studies, some report similar values of $E_a(\sigma)$ and $E_a(f_{max})$, whereas others report very different values, as listed in Table 1.

Table 1. Comparison of $E_a(\sigma)$ and $E_a(f_{max})$ for several materials from literature.

Material	$E_a(\sigma)$ / eV	$E_a(f_{max})$ / eV
$(Zr_{0.6}Ce_{0.4})_{0.92}(Y_2O_3)_{0.08}$ [10]	1.08 ± 0.01	1.07 ± 0.03
$SrFe_{1/2}Nb_{1/2}O_3$ [11]	0.272	0.267
$(Na_{0.75}Bi_{0.25})(Mn_{0.25}Nb_{0.75})O_3$ [12]	0.38	0.40
$Ce_{0.9}Gd_{0.05}Nd_{0.05}O_{1.95}$ [13]	0.976 ± 0.017	0.983 ± 0.019
Bi_5NbO_{10} [14]	0.94 ± 0.02	0.85 ± 0.03
$Bi_5Ti_{1.5}W_{1.5}O_{15}$ [15]	0.39	0.76
$LaMnO_3$ [16]	~ 0.17	0.05

There are different interpretations of the physical meaning of $E_a(f_{max})$. S. Anirban *et al.* attribute $E_a(f_{max})$ in Nd-doped GDC to the migration or reorientation energy of oxygen vacancies.[13] Hou *et al.* attribute $E_a(f_{max})$ in Bi_5NbO_{10} to a detrapping or relaxation energy of oxygen ions, and the difference between $E_a(\sigma)$ and $E_a(f_{max})$ to the energy for mobility of the free ions.[14] A. Karmakar *et al.* suggested a polaronic relaxation process in $LaMn_{1-x}Fe_xO_3$ based on the value of $E_a(f_{max})$.[16] Although various interpretations are possible, it is clear that $E_a(f_{max})$, or the difference between $E_a(f_{max})$ and $E_a(\sigma)$, may provide useful/additional information regarding conduction and/or relaxation mechanisms as f_{max} combines the contributions from conduction (R) and polarisation (C) processes according to Eq.(3). In the case of ferroelectric and ferroelectric-relaxor materials, the permittivity (and therefore C) has a strong temperature dependence, especially near T_C (ferroelectrics) or T_m (relaxors) where a maximum in C occurs which may result in different $E_a(f_{max})$ and $E_a(\sigma)$ values, and therefore requires further consideration.

There are many different types of ferroelectric materials including, hydrogen bonded salts, complex oxides and polymers. Oxide-based ferroelectric ceramics have significant technological importance and are based on many different but well known structural types including perovskite, illmenite, tungsten bronze and Aurivillius. Here we focus mainly on perovskite- and Aurivillius-type ceramics, to illustrate trends in $E_a(\sigma)$ and $E_a(f_{max})$ values for ferroelectric materials from impedance spectroscopy. The materials selected below were based on the following criteria: i) they are of particular interest due to their commercial applications; ii) they have representative permittivity-temperature profiles, i.e., sharp or broad C peak at T_C or T_m; iii) they are suitable for an f_{max} study by impedance spectroscopy, i.e., neither too conductive ($\sigma > 10^{-2}$ S cm^{-1}) nor too insulating ($\sigma < 10^{-8}$ S cm^{-1}) near T_C or T_m.

1) Perovskite lead zirconate titanate, PZT, is the most widely studied and commonly used piezoelectric/ferroelectric ceramic. The properties of PZT can be tuned flexibly by chemical doping to meet the requirements for different applications. Acceptor doping generates oxygen vacancies to prohibit domain wall motion, resulting in "hard" PZT for high-power applications such as ultrasonic cleaning, transformers and sonar technologies.[17] Donor doping induces cation vacancies to facilitate domain wall motion resulting in "soft" PZTs, which are typically used in sensors or actuators.[18] We present results for both "soft" (5H) and "hard" (4A) PZT.
2) $Na_{0.5}Bi_{0.5}TiO_3$ (NBT) is a complex perovskite which is considered as a promising lead-free piezoelectric/ferroelectric material to replace PZT. NBT shows relaxor behaviour with a broad and frequency-dependent permittivity, as well as a diffusive phase transformation.[19] Recent studies show NBT can present different types of electrical behaviour depending on the A-site Na or Bi nonstoichiometry, e.g., Bi-deficient NBT, nominal $Na_{0.5}Bi_{0.49}TiO_{2.985}$ ($NB_{0.49}T$), shows a predominant oxide-ion conduction mechanism with an oxide-ion transport number close to unity, whereas Bi-excess NBT, nominal $Na_{0.5}Bi_{0.51}TiO_{3.015}$ ($NB_{0.51}T$) shows predominant *n*-type electronic conduction behaviour with an oxide-ion transport number close to zero. [3-5] Details of the defect chemistry and electrical properties of NBT can be found in a recent review.[6] Results are presented here for both types of NBT.
3) Aurivillius phases, with a general formula of $(Bi_2O_2)(A_{m-1}B_mO_{3m+1})$ ($1 \le m \le 5$), represent a family of ferroelectric materials with layered bismuth-based structures.[20-22] This family of phases is built up by intercalating pseudo-perovskite $(A_{m-1}B_mO_{3m+1})^{2-}$ slabs between $(Bi_2O_2)^{2+}$ layers along the c axis.[20-22] These compounds have attracted significant attention due to their potential applications in high temperature lead-free piezoelectric devices or in ferroelectric random access memories.[23] Here we present results for $Bi_{2.5}Na_{0.5}Nb_2O_9$ (m = 2), $Bi_{2.5}Na_{1.5}Nb_3O_{12}$ (m = 3) and $Na_{0.5}Bi_{4.5}Ti_4O_{15}$ (m = 4).
4) Non-ferroelectric oxide-ion conductors, 8 mol% yttria-stabilised zirconia (8YSZ) and Dy,W-codoped Bi_2O_3 (8D4WSB) are included to represent electroceramics with near temperature-independent permittivity (and therefore temperature-independent C) values for comparison with the ferroelectric materials described above.

View Article Online DOI: 10.1039/C8TC03014A

Published on 13 August 2018. Downloaded by University of Sheffield on 8/14/2018 9:16:36 AM.

Journal of Materials Chemistry C Accepted Manuscript

This journal is © The Royal Society of Chemistry 20xx

Please do not adjust margins

View Article Online
DOI: 10.1039/C8TC03114A

Published on 13 August 2018. Downloaded by University of Sheffield on 8/14/2018 9:16:36 AM.

Journal of Materials Chemistry C Accepted Manuscript

Prior to presenting the experimental results, numerical simulations are used to investigate combinations of different logσ – T^{-1} and ε_r – T profiles on the logf_{max} – T^{-1} relationship and $E_a(f_{max})$. Both experimental and simulation results show that the ε_r – T profile and the temperature range relative to a T_m (temperature at which the permittivity reaches its maximum and could be T_C or T_M) are critical to the logf_{max} – T^{-1} relationship and values of $E_a(f_{max})$. We conclude that using $E_a(f_{max})$ to represent the activation energy for bulk electrical conduction (and therefore to discuss the conduction mechanism(s)) in ferroelectric ceramics is very limited in its application, and if employed, should be used with caution. The use of $E_a(\sigma)$ is recommended.

Experimental

Sample preparation and characterisation

8 mol% Y_2O_3- stabilised zirconia (8YSZ) pellets were prepared from commercially available powder (TZ-8T, Tosoh, Japan). The raw powder was ball milled overnight, dried, sieved, pressed into pellets and sintered at 1773 K for 4 h. $(BiO_{1.5})_{0.88}(DyO_{1.5})_{0.08}(WO_3)_{0.04}$ (8D4WSB), $Na_{0.5}Bi_{0.5}TiO_3$ (NBT), $Na_{0.5}Bi_{4.5}Ti_4O_{15}$, $Bi_{2.5}Na_{0.5}Nb_2O_9$ and $Bi_{2.5}Na_{1.5}Nb_3O_{12}$ were prepared by the solid-state reaction method using Bi_2O_3 (99.9%, Acros Organics, USA), Dy_2O_3 (99.9%, Stanford Advanced Materials, USA), WO_3 (99.8%, Alfa Aesar, UK), Na_2CO_3 (99.5%, Fisher chemical, UK), TiO_2 (99.9%, Sigma Aldrich, UK) and Nb_2O_5 (99.9%, Sigma Aldrich, UK) as starting materials. Before weighing, the above raw powders were pre-dried (573 K or 1173 K for 8 h, as appropriate). Appropriate amounts of each precursor were weighed and mixed thoroughly in iso-propanol using yttria-stabilised zirconia grinding media for 6 hours. The mixture was dried overnight at 358 K, sieved and then calcined at 1073 K for 2 hours. The resultant powders were subjected to a second round of ball milling, drying, sieving and calcination and subsequently to a final, third round of ball milling and sieving. The products were compacted into pellets by uni-axial cold pressing and then isostatic pressing at 200 MPa, followed by sintering at 1198 K for 2 h (8D4WSB), 1150 °C for 2 h (NBT and $Na_{0.5}Bi_{4.5}Ti_4O_{15}$), 1423 K for 8 h ($Bi_{2.5}Na_{0.5}Nb_2O_9$ and $Bi_{2.5}Na_{1.5}Nb_3O_{12}$). Prior to sintering, pellets were embedded in sacrificial powder of the same composition to minimise volatilisation. Lead zirconate titanate (PZT) samples (4A and 5H) are commercially available pellets with silver electrodes (Morgan Advanced Materials, UK). All samples that we prepared are phase pure by XRD (STOE STADI-P diffractometer, STOE & Cie GmbH, Darmstadt, Germany) and dense (> 95% of theoretical density). XRD patterns and lattice parameters obtained from Rietveld refinements are provided in supplementary materials as Fig.S1. Electrical properties were obtained from ac impedance spectroscopy using an Agilent E4980A impedance analyser (Agilent Technologies, Palo Alto, CA; frequency range 1 MHz to 20 Hz) and/or a Solartron 1260 system (Solartron Analytical, UK; frequency range 1 MHz to 0.01 Hz). Dielectric properties were measured using an LCR meter (Agilent E4980 Precision LCR Meter, Agilent Technologies) with an applied ac voltage of 100 mV. Data points were collected every 60 s over a proper temperature range using a non-inductively wound tube furnace at a ramping rate of 1 K min^{-1}. Before measurements, Au paste was painted to cover both surfaces of the pellets and then fired at 1123 K for 2 h to serve as electrodes.

Impedance data analysis

Bulk conductivity and permittivity values were obtained from impedance data by two methods, i.e., equivalent circuit fitting and calculation from the large M'' Debye peak associated with the bulk response. In equivalent circuit fitting, each response in the Z* plot was fitted by a parallel R-CPE element. The impedance of a CPE, Z_{CPE}, is given by[9, 24, 25]

$$Z_{CPE} = \frac{1}{Q(j\omega)^n} = Q^{-1}\omega^{-n}\left[\cos\left(\frac{n\pi}{2}\right) + jsin\left(\frac{n\pi}{2}\right)\right], \quad (5)$$

where Q is a parameter independent of frequency and n is an exponential factor. An equivalent capacitance, C, of the CPE can be calculated by[26]

$$C = R^{(1-n)/n}Q^{1/n}. \quad (6)$$

The obtained R and C for the bulk response are converted to conductivity and permittivity by

$$\sigma_b = \frac{1}{R_b}\frac{4t}{\pi D^2}, \quad (7a)$$

$$\varepsilon_r = \frac{C}{\varepsilon_0}\frac{4t}{\pi D^2}, \quad (7b)$$

where t and D are the thickness and diameter of the pellet, respectively; ε_0 is the permittivity of free space (8.85×10^{-14} F cm^{-1}). Alternatively, R and C can be calculated from the M''-log$f$ spectroscopic plot from the M'' peak value, M_{max}'' and the characteristic frequency, f_{max}, according to

$$R = \frac{M''_{max}}{\pi f_{max}}. \quad (8a)$$

$$C = \frac{1}{2M''_{max}}, \quad (8b)$$

R and C values are converted to σ_b and ε_r using Eqs.7a and 7b. In this script, σ_b and ε_r are calculated from both methods.

Numerical Simulations

Here we generate two series of logσ – T^{-1} profiles according to Eq.1. A): In the temperature range between T_1 and T_2, log(σ/σ_0) shows a straight line with different slopes, corresponding to $E_a(\sigma)$ of 0.5 - 2.0 eV, respectively (Fig.1a) and B): in the temperature range between T_1 and T_3, log(σ/σ_0) shows a change of $E_a(\sigma)$ at T_2, from 0.5 eV between T_2 and T_3 to 1.0, 1.5 and 2.0 eV between T_1 and T_2 (Fig.1b). For the ε_r – T profile, we simplify it to a symmetric peak with a maximum at T_m. For ferroelectrics, above the Curie temperature the permittivity obeys the Curie-Weiss law and can be described by

$$\frac{1}{\varepsilon_r} = \delta T + A. \quad (9)$$

Here we vary the δ value from 2×10^{-8} (δ_1) to 1×10^{-5} (δ_7) to change the slope of the ε_r^{-1} -T relationship, and consequently the ε_r - T profile above T_m. The ε_r - T profile below the Curie temperature is generated as the mirror symmetry of its counterpart above T_m. The larger δ, the sharper the permittivity peak. A temperature-independent permittivity is also included for comparison (δ_0). Using the logσ - T^{-1} and ε_r - T profiles, the characteristic frequency f_{max} is calculated according to

$$f_{max} = \frac{1}{2\pi RC} = \frac{1}{2\pi\varepsilon_0}\frac{\sigma}{\varepsilon_r}. \quad (10)$$

Please do not adjust margins

View Article Online
DOI: 10.1039/C8TC03211J

Published on 13 August 2018. Downloaded by University of Sheffield on 8/14/2018 9:16:36 AM.

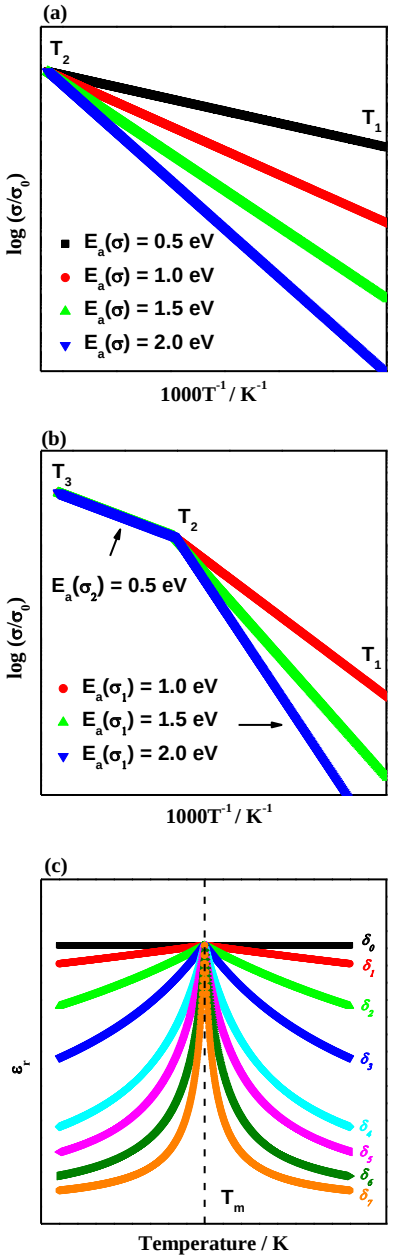

Fig.1 Conductivity and permittivity-temperature profiles used for simulation. (a) Arrhenius plots with E_a varying from 0.5 to 2.0 eV in a temperature range between T_1 and T_2. (b) Arrhenius plot showing a change of E_a at T_2 in the temperature range between T_1 and T_3. Above T_2, $E_a(\sigma_2)$ is fixed at 0.5 eV. Below T_2, $E_a(\sigma_2)$ varies from 1.0 to 2.0 eV. (c) ε_r-T profiles with different δ values: $\delta_0 = 0$; $\delta_1 = 5.0 \times 10^{-8}$ K^{-1}; $\delta_2 = 2.0 \times 10^{-7}$ K^{-1}; $\delta_3 = 5.0 \times 10^{-7}$ K^{-1}; $\delta_4 = 1.5 \times 10^{-6}$ K^{-1}; $\delta_5 = 2.5 \times 10^{-6}$ K^{-1}; $\delta_6 = 5.0 \times 10^{-6}$ K^{-1}; $\delta_7 = 1.0 \times 10^{-5}$ K^{-1}.

Part A, Constant $E_a(\sigma)$ in the measured temperature range, T_1 to T_2.

First, we consider a constant $E_a(\sigma)$, i.e., 0.5 eV, over the temperature range of interest. This can be divided into two cases to represent; (1) where impedance data are collected over a temperature range that is either much higher or lower than T_m, and (2) across a range that includes T_m.

1) $T_2 > T_1 >> T_m$ or $T_1 < T_2 << T_m$

If T_m is far outside the temperature range investigated, i.e., T_1 is 100 K higher than T_m or T_2 is 100 K lower than T_m, $\log f_{max}$ shows a linear relationship with T^{-1}, Fig.2a and b.

2) $T_1 < T_m < T_2$

If the ferro- to para-electric phase transition occurs within the temperature range investigated, i.e., T_m is between T_1 and T_2, the $\log f_{max}$ - T^{-1} relationship depends on δ. When δ is small (δ_0 to δ_2), $\log f_{max}$ still shows a linear relationship with T^{-1}; with increasing δ, $\log f_{max}$ starts to deviate from a linear relationship with T^{-1} with increasing δ, especially near the vicinity of T_m, Fig.2c.

For the linear $\log f_{max}$ - T^{-1} relationship in Fig.2a and b, we calculated the associated $E_a(f_{max})$, as well as the difference between $E_a(f_{max})$ and $E_a(\sigma)$. Here we define a parameter, ΔE_a, according to

$$\Delta E_a = \frac{E_a(f_{max}) - E_a(\sigma)}{E_a(\sigma)} \times 100\%, \quad (11)$$

and plotted it as a function of δ, Fig.2d. It shows that when $T_1 >> T_m$, the activation energy calculated from time constant (via $\log f_{max}$) tends to be overestimated and when $T_2 << T_m$ it tends to be underestimated. Higher δ values lead to larger deviations. ΔE_a is also dependent on $E_a(\sigma)$: with a smaller $E_a(\sigma)$, i.e., 0.5 eV, the deviation between $E_a(f_{max})$ and $E_a(\sigma)$ is much more significant than with a larger $E_a(\sigma)$, i.e., 2.0 eV. Furthermore, ΔE_a is much higher when $T_1 >> T_m$ than when $T_2 << T_m$. For example, for $E_a(\sigma)$ = 0.5 eV, ΔE_a can be over 50% when $T_1 >> T_m$, but it is less than 20% when $T_2 << T_m$. This suggests the permittivity-temperature profile plays a key role on the $\log f_{max}$ - T^{-1} relationship, and therefore the value of $E_a(f_{max})$. A sharp peak in the ε_r – T profile can lead to an observable distortion of the $\log f_{max}$ - T^{-1} plot at the transition temperature, whereas a broad ε_r peak has a smaller influence on the $\log f_{max}$- T^{-1} plot but can lead to either an over- or under-estimation of E_a.

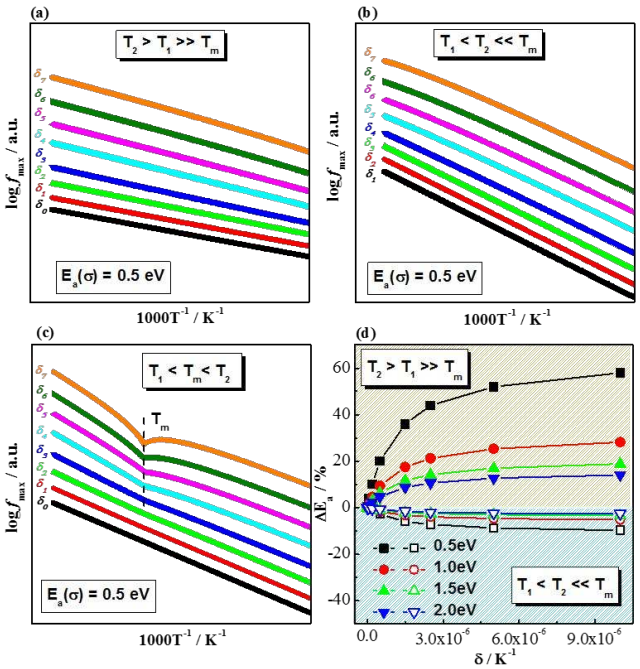

Fig.2 (a)-(c) $\log f_{max}$ – T^{-1} plot in the case of $T_2 > T_1 >> T_m$, $T_1 < T_2 << T_m$ and $T_1 < T_m < T_2$, respectively. (d) ΔE_a as a function of δ for $E_a(\sigma)$ = 0.5, 1.0, 1.5 and 2.0 eV in the cases of $T_2 > T_1 >> T_m$ and $T_m << T_1 < T_2$.

Journal of Materials Chemistry C Accepted Manuscript

This journal is © The Royal Society of Chemistry 20xx

Please do not adjust margins

View Article Online
DOI: 10.1039/C8TC03014A

Published on 13 August 2018. Downloaded by University of Sheffield on 8/14/2018 9:16:36 AM.

Part B, Change of $E_a(\sigma)$ in the measured temperature range

If there is a change of $E_a(\sigma)$ over the temperature range investigated, the Arrhenius plot used for simulation is shown in Fig.1b: over T_1 to T_3, $E_a(\sigma)$ changes from $E_a(\sigma_1)$ = 1.0, 1.5 or 2.0 eV (between T_1 and T_2, low temperature (LT) region) to $E_a(\sigma_2)$ = 0.5 eV (between T_2 and T_3, high temperature (HT) region). Using $E_a(\sigma_1)$ = 1.0 eV as an example, in the cases of:

1) $T_3 > T_2 > T_1 >> T_m$ (Fig.3a)

The $\log f_{max}$ - T^{-1} plot shows a change of slope at T_2 for all δ. Both below and above T_2, $\log f_{max}$ shows a linear relationship with T^{-1}, Fig.3a.

2) $T_1 < T_2 < T_3 << T_m$ (Fig.3b)

The $\log f_{max}$ - T^{-1} plot still shows a change of slope at T_2 for all δ. Below T_2, $\log f_{max}$ shows a linear relationship with T^{-1}. Above T_2, $\log f_{max}$ with larger δ values (δ_6 to δ_8) deviates from a linear relationship with T^{-1} at higher temperatures, as indicated by the circle in Fig.3b.

3) $T_1 < T_2 = T_m < T_3$ (Fig.3c)

If the change of $E_a(\sigma)$ occurs at the same temperature as the phase transition temperature, the $\log f_{max}$ - T^{-1} plot shows various features depending on δ. For smaller δ values (e.g., δ_0 to δ_3), the $\log f_{max}$ - T^{-1} plot shows a change of slope at T_2. Both below and above T_2, $\log f_{max}$ shows a linear relationship with T^{-1}. With increasing δ (e.g., δ_4 and δ_5), the change of E_a at T_2 cannot be observed and the $\log f_{max}$- T^{-1} plot shows a linear relationship with T^{-1} between T_1 and T_3. With a further increase in δ (δ_6 and δ_7), $\log f_{max}$- T^{-1} shows a distortion at T_2 (=T_m), Fig.3c.

4) $T_1 < T_2 < T_m < T_3$ or $T_1 < T_m < T_2 < T_3$ (Fig.3d and e)

If the change of $E_a(\sigma)$ and phase transition occur at different temperatures, the $\log f_{max}$ - T^{-1} relationship is also dependent on δ and can be complicated. In general, with small δ values (δ_0 to δ_3), the $\log f_{max}$ - T^{-1} plot presents similar behaviour to the logσ – T^{-1} plot and only one kink at T_2 can be observed. With increasing δ, the distortion at T_m becomes increasing obvious to give multiple features on the $\log f_{max}$ - T^{-1} plot.

For the linear $\log f_{max}$ - T^{-1} relationship in the HT and LT regions in Fig.3a and b, we also calculated the associated $E_a(f_{max})$ and ΔE_a values. As shown in Fig.3f, if the lowest temperature investigated is much higher than the phase transition temperature, i.e., $T_1 >> T_m$, using the time constant related parameter f_{max} tends to overestimate E_a for both the HT and LT regions, and it shows a more significant effect on the HT region. ΔE_a is also dependent on δ: larger δ values generate larger ΔE_a. Furthermore, the lower $E_a(\sigma_1)$, the larger ΔE_a for the LT region, whereas $E_a(\sigma_1)$ has no impact on ΔE_a for the HT region. If the highest temperature investigated is much lower than the phase transition temperature, i.e., $T_3 << T_m$, using f_{max} tends to underestimate E_a for both the HT and LT regions, and it shows a more significant effect on the HT region. The larger δ and the smaller $E_a(\sigma_1)$ values, the larger $|\Delta E_a|$.

The above numerical simulations suggest the permittivity-temperature profile, as well as the measurement temperature range relative to the phase transition temperature, has a large effect on the $\log f_{max}$ – T^{-1} relationship, and consequently $E_a(f_{max})$. If the phase transition temperature is far outside the temperature range investigated, the $\log f_{max}$ – T^{-1} plot usually shows linear behaviour similar to the logσ – T^{-1} plot but it can overestimate or underestimate the activation energy. If the phase transition temperature is within the temperature range investigated, depending on the permittivity-temperature profile, the $\log f_{max}$ – T^{-1} plot can be significantly different from the logσ – T^{-1} plot and consequently give misleading information. For example, although logσ shows a linear relationship with T^{-1}, $\log f_{max}$ can show a change of E_a with certain ε_r – T profiles (eg. Fig.2c, δ_4); or although the logσ - T^{-1} plot shows a kink, $\log f_{max}$ can show a linear relationship with T^{-1} for certain ε_r – T profiles (eg. Fig.3c, δ_4 and δ_5).

In practice, real ε_r – T profiles can be considerably more complicated than those used in these simulations, i.e. permittivity is not symmetric around T_m and often contains multiple peaks. However, it is clear that $E_a(f_{max})$ is only equal to $E_a(\sigma)$ when ε_r is temperature-independent, which is not the case for ferroelectric materials. The sharper the permittivity peak, the larger the deviation of $E_a(f_{max})$ from $E_a(\sigma)$.

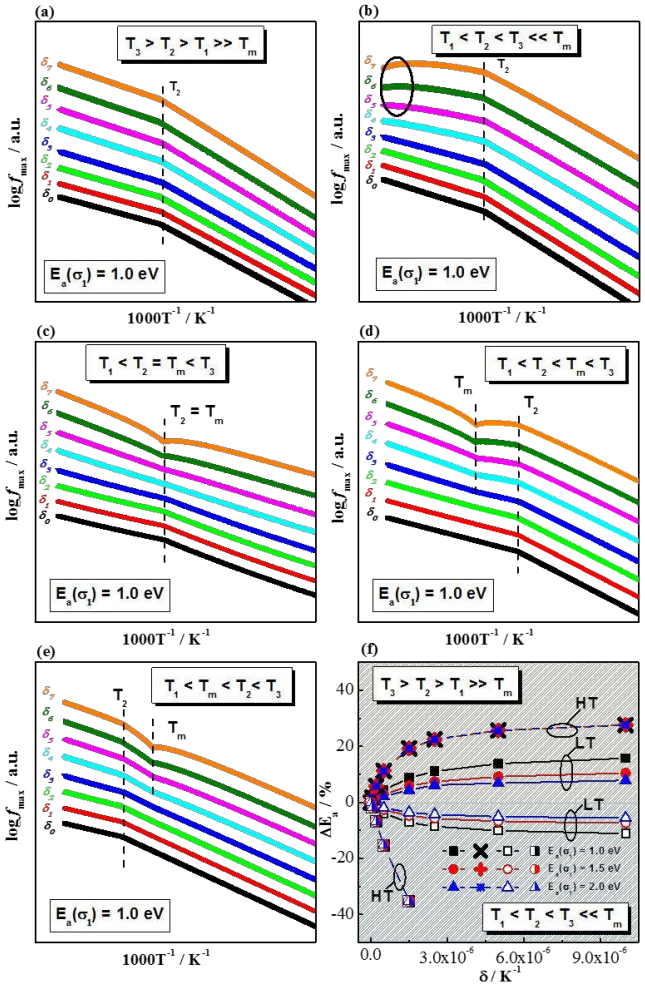

Fig.3 $\log f_{max}$ – T^{-1} plot in the cases of (a) $T_3 > T_2 > T_1 >> T_m$; (b) $T_1 < T_2 < T_3 << T_m$; (c) $T_1 < T_2 = T_m < T_3$; (d) $T_1 < T_2 < T_m < T_3$; (e) $T_1 < T_m < T_2 < T_3$. (f) ΔE_a as a function of δ for $E_a(\sigma_1)$ = 1.0, 1.5 and 2 eV in the cases of $T_3 > T_2 > T_1 >> T_m$ and $T_1 < T_2 < T_3 << T_m$.

Journal of Materials Chemistry C Accepted Manuscript

Please do not adjust margins

View Article Online
DOI: 10.1039/C8TC03011A

Published on 13 August 2018. Downloaded by University of Sheffield on 8/14/2018 9:16:36 AM.

Experimental results

The experimental results are subdivided into two sections. The first section considers materials where the bulk conductivity has a single activation energy over the measured temperature range and the second section considers examples where there is a change in the value of the activation energy associated with the bulk conductivity within the measured temperature range. The permittivity-temperature and dielectric loss-temperature profiles for the ferroelectric materials were measured using an LCR meter from room temperature to 873 or 1073 K and are shown in the supplementary information (Figs. S2-S8). The shaded regions in the permittivity plots therein indicate the temperature range over which impedance spectroscopy data could be obtained for these samples and is the focus of the results section.

Part A, Materials with constant E_a

1) 8YSZ and 8D4WSB (δ_0)

A typical Z* plot for 8YSZ shows three responses, from high to low frequency (left to right), corresponding to bulk, grain boundary and electrode effects, respectively, Fig.4a. The impedance spectra of 8YSZ were fitted by an equivalent circuit of three R-CPE in series connection (inset in Fig.4a) with the bulk resistance (subsequently converted to conductivity) being associated with the large arc and element R_1-CPE_1 in the equivalent circuit. The M''-log$f$ spectroscopic plot of 8YSZ (Fig.4b) shows a single Debye peak, corresponding to the bulk response as it has much lower capacitance (orders of magnitude lower) than the responses from grain boundary and the electrode effect. With increasing temperature, the M'' peak shifts to higher frequency but the peak height remains unchanged. As the peak height is proportional to the reciprocal of the bulk capacitance, the constant peak height indicates a temperature-independent capacitance, and therefore a temperature-independent permittivity, as shown in Fig.4c. Arrhenius plots for the bulk conductivity, σ_b, (obtained from equivalent circuit fitting and from the M'' spectroscopic plots) and f_{max} (from M'' spectroscopic plots) are shown in Fig.4d. The activation energies calculated from the linear fitting of logσ_b - T^{-1} and logf_{max} - T^{-1} relationship are identical with a value of 1.07 eV. 8D4WSB showed similar behaviour with the results presented in Fig.S9 in SI with $E_a(\sigma_b)$ and $E_a(f_{max})$ values of 0.93 eV.

2) $Bi_{2.5}Na_{1.5}Nb_3O_{12}$ (small δ, i.e., δ_1- δ_2; $T_1 < T_m < T_2$, see Fig.S2 for ε_r –T profile)

Z* plots for $Bi_{2.5}Na_{1.5}Nb_3O_{12}$ showed a single arc associated with a bulk response and could be fitted by an equivalent circuit of one R-CPE element, Fig.5a and its inset. The M''-log$f$ spectroscopic plot shows a single Debye peak, which shifts to higher frequency with increasing temperature, Fig.5b. The M'' Debye peak height shows little variation from ~ 823 to 948 K before it starts to increase significantly at higher temperatures up to 1073 K. Consequently, the permittivity-temperature profile is quite flat from 823 to 948 K and then it starts to decrease with temperature, Fig.5c. Linear fitting of the logσ_b - T^{-1} and logf_{max} - T^{-1} relationships give E_a values of 1.63 and 1.69 eV, respectively, Fig.5d.

3) "soft" PZT 5H and $NB_{0.51}T$ (large δ, i.e., $\delta_5 - \delta_7$, $T_2 > T_1 >> T_m$, see Fig.S3 and Fig.S4 for ε_r –T profile, respectively)

Z* plots for PZT 5H also showed a single arc associated with a bulk response which could be fitted by a single R-CPE element, Fig.6a and its inset. The single, Debye peak in the M''-log$f$ spectroscopic plots shifts to higher frequency with increasing temperature with a continuous increase in peak height, Fig.6b, and consequently a continuous decrease in permittivity from 723 to 923 K, Fig.6c. Arrhenius plots for σ_b and f_{max} both show a linear relationship with T^{-1} but with different activation energies, i.e., $E_a(\sigma_b)$ ~ 1.26 eV and $E_a(f_{max})$ ~ 1.47 eV, Fig.6d. $NB_{0.51}T$ showed similar impedance behaviour with the results presented in Fig.S10 in SI with $E_a(\sigma_b)$ ~ 1.71 eV and $E_a(f_{max})$ ~ 1.95 eV, Fig.S10(d).

4) $Bi_{2.5}Na_{0.5}Nb_2O_9$ (intermediate or large δ, i.e., $\delta_3 - \delta_7$, $T_1 < T_2 << T_m$, see Fig.S5 for ε_r –T profile)

Z* plots for $Bi_{2.5}Na_{0.5}Nb_2O_9$ showed a single arc associated with a bulk response and could be fitted by an equivalent circuit of one R-CPE element, Fig.7a and its inset. The M''-log$f$ spectroscopic plots show a single Debye peak, which shifts to higher frequency with increasing temperature, Fig.7b. The peak height remains relatively constant from 823 to 873 K, and then decreases rapidly with increasing temperature, Fig.7b. Accordingly, the permittivity shows very little change between 823 and 873 K, and then starts to increase with increasing temperature, Fig.7c. Arrhenius plots for σ_b and f_{max} both show a linear relationship with T^{-1} but with different activation energies, i.e., $E_a(\sigma_b)$ ~ 1.83 eV and $E_a(f_{max})$ ~ 1.49 eV, Fig.7d.

5) "hard" PZT 4A and $Na_{0.5}Bi_{4.5}Ti_4O_{15}$ (large δ, i.e., $\delta_5 - \delta_7$, $T_1 < T_m < T_2$, see Fig.S6 and Fig.S7 for ε_r –T profile, respectively)

Z* plots of hard PZT showed a single arc associated with a bulk response which can be fitted by a single R-CPE element, Fig.8a and its inset. The M''-log$f$ spectroscopic plots show a single peak, corresponding to the bulk response, which shifts to higher frequency with increasing temperature, Fig.8b. The M'' peak height initially decreases significantly with increasing temperature, reaching its minimum at ~ 568 K, and then increases up to the highest measured temperature of 673 K. Consequently, the permittivity increases rapidly from ~ 2500 at 473 K to its peak value of ~ 15,000 at 568 K, and then decreases rapidly to ~ 2500 at 673 K, Fig.8c. Arrhenius plots for σ_b show a linear relationship with T^{-1} to give $E_a(\sigma_b)$ ~ 1.08 eV. In contrast, an Arrhenius plot for logf_{max} shows complex behaviour. It can be divided into three regions: below 533 K or above 593 K, logf_{max} linearly decreases with increasing T^{-1} with $E_a(f_{max})$ ~ 0.85 eV and 1.73 eV respectively; between 533 and 593 K, logf_{max} - T^{-1} is curved and shows a downward bend, Fig.8d. Similar behaviour with a non-linear logf_{max} – T^{-1} relationship near T_m with a more pronounced downward bend is observed from the analysis of impedance data for $Na_{0.5}Bi_{4.5}Ti_4O_{15}$ shown in Fig.S11 in the SI.

Journal of Materials Chemistry C Accepted Manuscript

This journal is © The Royal Society of Chemistry 20xx

Please do not adjust margins

View Article Online
DOI: 10.1039/C8TC03011A

Published on 13 August 2018. Downloaded by University of Sheffield on 8/14/2018 9:16:36 AM.

Journal of Materials Chemistry C Accepted Manuscript

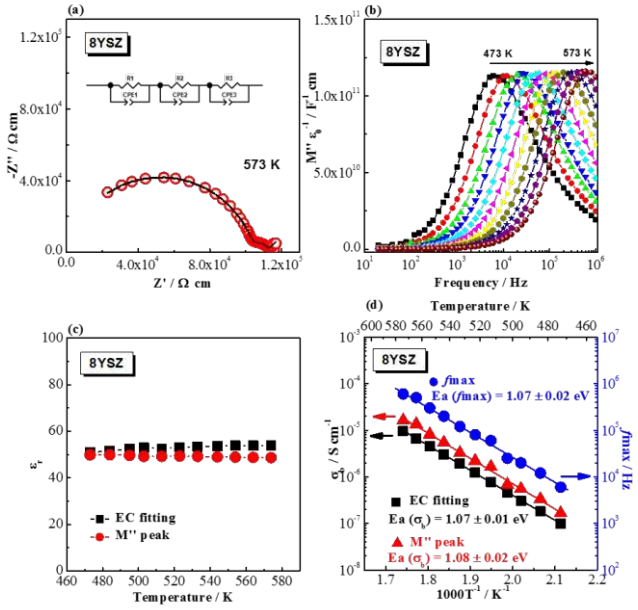

Fig. 4 (a) Z* plot for 8YSZ measured at 573 K. Red open circles are the experimental data and the black line is the fitting curve using the equivalent circuit (EC) shown in the inset; (b) M''-log*f* plots from 473 to 573 K with an interval of 10 K; (c) Relative permittivity as a function of temperature; and (d) Arrhenius plots for the bulk conductivity, σ_b, calculated by both EC fitting and M'' peak, and the characteristic frequency, f_{max} and their associated activation energies $E_a(\sigma_b)$ and $E_a(f_{max})$, respectively.

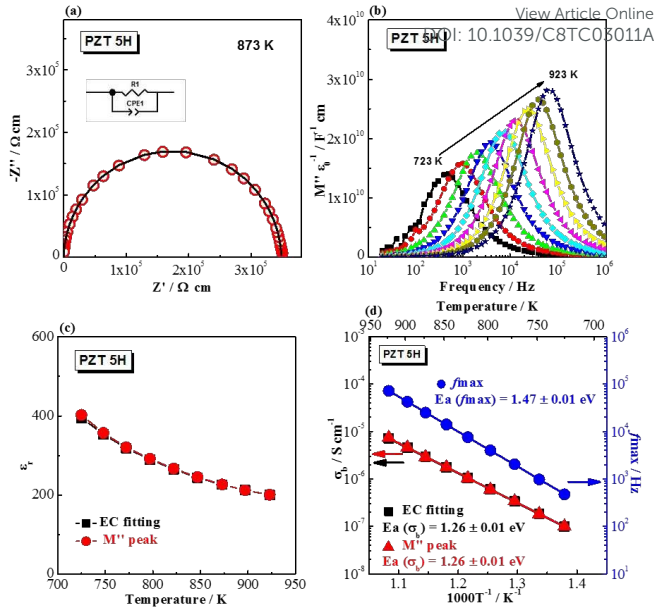

Fig.6 (a) Z* plot for PZT 5H measured at 873 K. Red open circles are the experimental data and the black line is the fitting curve using the equivalent circuit (EC) shown in the inset figure; (b) M''-log*f* plots from 723 to 923 K at an interval of 25 K; (c) Relative permittivity as a function of temperature; and (d) Arrhenius plots for the bulk conductivity, σ_b, and the time constant related parameter f_{max} and their associated activation energies $E_a(\sigma_b)$ and $E_a(f_{max})$, respectively.

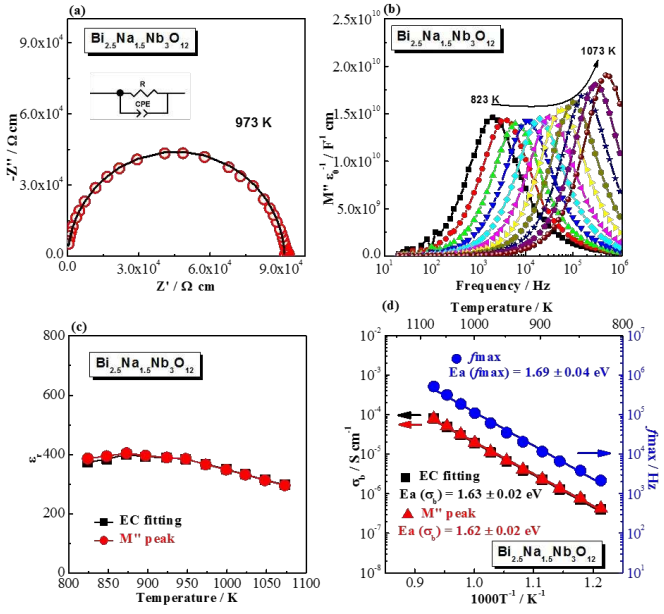

Fig.5 (a) Z* plot for $Bi_{2.5}Na_{1.5}Nb_3O_{12}$ measured at 973 K. Red open circles are the experimental data and the black line is the fitting curve using the equivalent circuit (EC) shown in the inset figure; (b) M''-log*f* plots from 823 to 1073 K at intervals of 25 K; (c) Relative permittivity as a function of temperature; and (d) Arrhenius plots for the bulk conductivity, σ_b, and the time constant related parameter f_{max} and their associated activation energies $E_a(\sigma_b)$ and $E_a(f_{max})$, respectively.

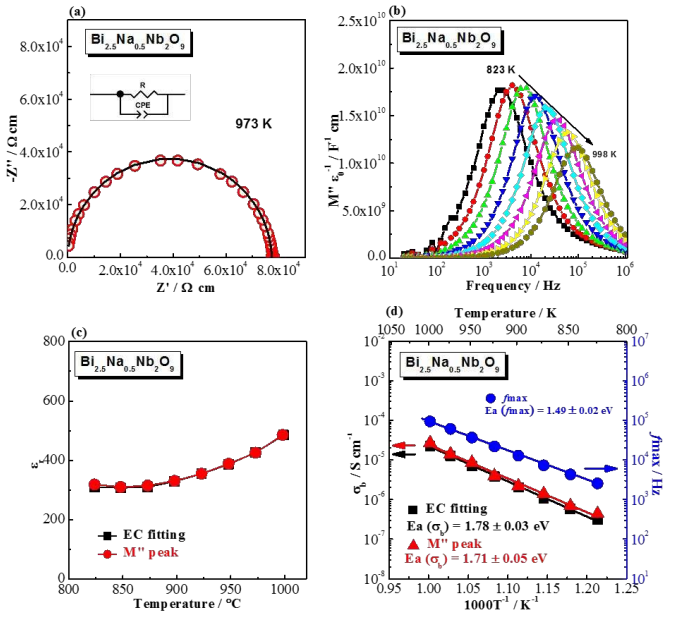

Fig.7 (a) Z* plot for $Bi_{2.5}Na_{0.5}Nb_2O_9$ measured at 973 K. Red open circles are the experimental data and the black line is the fitting curve using the equivalent circuit (EC) shown in the inset figure; (b) M''-log*f* plots from 823 to 998 K at intervals of 25 K; (c) Relative permittivity as a function of temperature; and (d) Arrhenius plots for the bulk conductivity, σ_b, and the time constant related parameter f_{max} and their associated activation energies $E_a(\sigma_b)$ and $E_a(f_{max})$, respectively.

Please do not adjust margins

View Article Online
DOI: 10.1039/C8TC03011A

Published on 13 August 2018. Downloaded by University of Sheffield on 8/14/2018 9:16:36 AM.

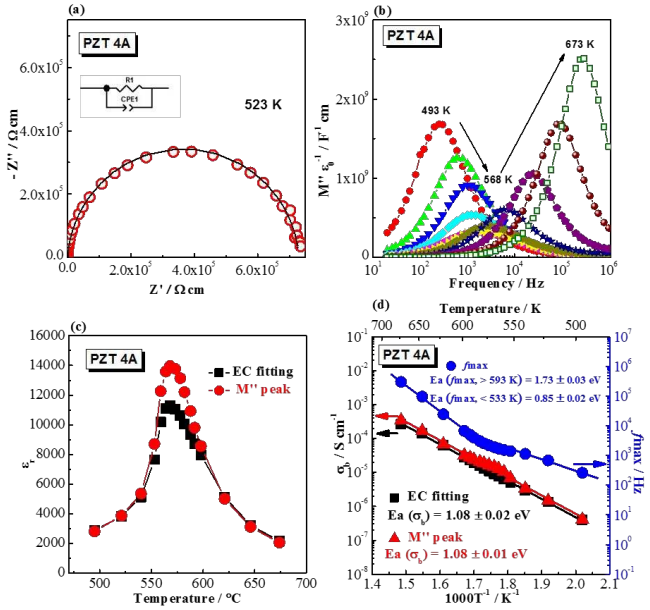

Fig.8 (a) Z* plot for PZT 4A measured at 523 K. Red open circles are the experimental data and the black line is the fitting curve using the equivalent circuit (EC) shown in the inset figure; (b) M''-log$f$ plots from 493 to 673 K at intervals of 25 K with smaller intervals in the range between 558 and 573 K ; (c) Relative permittivity as a function of temperature; and (d) Arrhenius plots for the bulk conductivity, σ_b, and the time constant related parameter f_{max} and their associated activation energies $E_a(\sigma_b)$ and $E_a(f_{max})$, respectively.

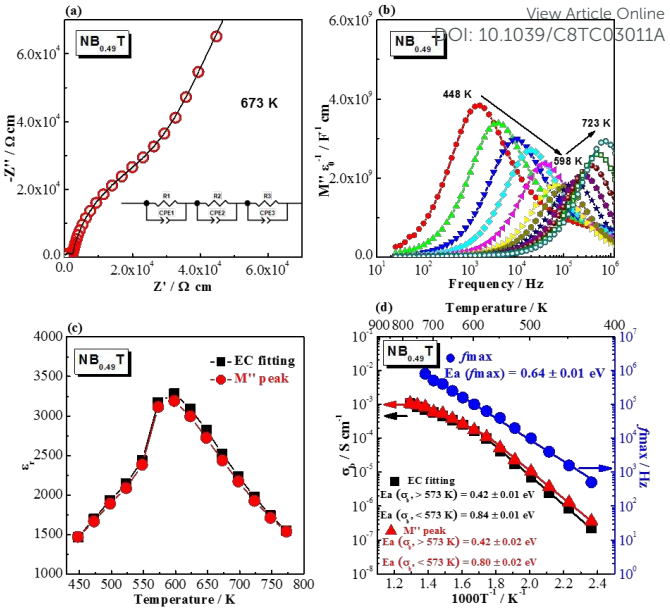

Fig. 9 (a) Z* plot for $NB_{0.49}T$ measured at 673 K. Red open circles are the experimental data and the black line is the fitting curve using the equivalent circuit (EC) shown in the inset figure; (b) M''-log$f$ plots from 448 to 723 K at intervals of 25 K; (c) Relative permittivity as a function of temperature; and (d) Arrhenius plots for the bulk conductivity, σ_b, and the time constant related parameter f_{max} and their associated activation energies $E_a(\sigma_b)$ and $E_a(f_{max})$, respectively.

Part B, Material with a change of E_a in the measured temperature range- $NB_{0.49}T$

Z* plots for oxide-ion conducting $NB_{0.49}T$ shows three arcs, from high to low frequency (left to right), corresponding to the responses from the bulk, grain boundary (GB) and electrode effects, respectively, Fig.9a. The origin of large impedance associated with the GB in $NB_{0.49}T$ is still under investigation but it may be associated with a space charge effect and/or impurity segregation, which are reported in many oxide-ion conductors such as YSZ and doped ceria.[27] The low-frequency spike associated with the electrode effect is a clear signature of ionic conduction.[3] The spectrum can be fitted using three R-CPE elements in series connection, inset in Fig.9a. The M''-log$f$ spectroscopic plot shows a single Debye peak, corresponding to the bulk response, which shifts to higher frequency with increasing temperature, Fig 9b. The M'' peak height decreases significantly with increasing temperature, reaching a minimum at 598 K, and then increases with increasing temperature. The permittivity of $NB_{0.49}T$, in the measured temperature range between 448 and 723 K, increases from ~ 1500 at 448 K to its peak value of ~ 3200 at 598 K, and then decrease to ~ 1500 at 723 K, Fig.9c. The bulk conductivity, σ_b, shows a change in activation energy, from ~ 0.85 eV at 448 – 573 K to 0.42 eV at 573 – 723 K, Fig.9d. The change of $E_a(\sigma_b)$ at ~ 573 K may be related to the coexistence of rhombohedral and tetragonal phases between 523 and 673 K, or a combination of defect associates and polymorphic phase transitions.[28-29] Nevertheless, the logf_{max} - T^{-1} plot shows a linear relationship with an activation energy of 0.64 eV, Fig.9d.

Discussion

1) Comparison between the simulations and experimental results

In this work we have investigated the use of two parameters commonly obtained from analysis of impedance spectroscopy data, i.e. bulk electrical conductivity (σ) and the characteristic frequency f_{max} related to the time constant of the bulk response, to assess their reliability in obtaining the activation energy for bulk conduction in ferroelectric materials over a range of temperature. The range may or may not include the permittivity peak at T_m associated with a ferro- to para-electric phase transition. Conduction mechanisms of these materials include predominant oxide-ion conduction (8YSZ, 8D4WSB, $NB_{0.49}T$), mixed ionic-electronic conduction (PZT 5H and $Na_{0.5}Bi_{4.5}Ti_4O_{15}$) and predominant electronic/hole conduction ($Bi_{2.5}Na_{1.5}Nb_3O_{12}$, $NB_{0.51}T$, $Bi_{2.5}Na_{0.5}Nb_2O_9$ and PZT4A). A summary of the conduction mechanisms and experimental results for the materials studied is given in Table 2. In contrast to non-ferroelectric materials such as 8YSZ and 8D4WSB, which show identical values for $E_a(\sigma)$ and $E_a(f_{max})$, most ferroelectric materials show different values of $E_a(\sigma)$ and $E_a(f_{max})$. Moreover, within certain temperature ranges, nonlinear behaviour between logf_{max} and T^{-1} is observed, e.g., for PZT 4A and $Na_{0.5}Bi_{4.5}Ti_4O_{15}$, see Fig.8 and Fig.S11, respectively. It is clear that the logf_{max} - T^{-1} relationship, and consequently the extracted value of $E_a(f_{max})$, is strongly dependent on logσ – T^{-1}, ε_r – T and the measured temperature range relative to T_m.

Journal of Materials Chemistry C Accepted Manuscript

This journal is © The Royal Society of Chemistry 20xx

Please do not adjust margins

View Article Online
DOI: 10.1039/C8TC03011A

Table 2. Summary of $E_a(\sigma)$ and $E_a(f_{max})$ for the materials investigated in this work. T_m and temperature range for impedance measurements for each material are also listed.

Material	Conduction mechanism/ charge carrier	T_m / K	Temperature range / K	$E_a(\sigma)$ / eV	$E_a(f_{max})$ / eV
8YSZ	Ionic, O^{2-} (ref.27)	-	473 – 573	1.07 ± 0.01	1.07 ± 0.02
8D4WSB	Ionic, O^{2-} (ref.30)	-	413 – 513	0.93 ± 0.01	0.93 ± 0.02
$Bi_{2.5}Na_{1.5}Nb_3O_{12}$	Electronic, *e* (Fig.S12)	~ 873, 943	823 – 1073	1.63 ± 0.02	1.69 ± 0.04
PZT 5H	Mixed, O^{2-} + h (Fig.S13)	~ 443	723 – 923	1.26 ± 0.01	1.47 ± 0.01
$NB_{0.51}T$	Electronic, *e* (ref.3)	~ 598	823 – 1073	1.71 ± 0.01	1.95 ± 0.02
$Bi_{2.5}Na_{0.5}Nb_2O_9$	Electronic, *e* (Fig.S14)	~ 1063	823 – 998	1.83 ± 0.02	1.49 ± 0.02
PZT 4A	Electronic, h (Fig. S15)	~ 568	473 – 673	1.07 ± 0.01	0.85 ± 0.02, T < 533 K Nonlinear, 533 < T < 593 K 1.73 ± 0.03, T > 593 K
$Na_{0.5}Bi_{4.5}Ti_4O_{15}$	Mixed, O^{2-} + *e* (Fig.S16)	~ 923	773 – 1073	1.54 ± 0.03	0.91 ± 0.02, T < 873 K Nonlinear, 873 < T < 973 K 1.94 ± 0.07, T > 973 K
$NB_{0.49}T$	Ionic, O^{2-} (ref.3)	~ 598	448 – 723	0.84 ± 0.01, T < 573 K 0.42 ± 0.01, T > 573 K	0.64 ± 0.01

The simulations show that $E_a(f_{max})$ equals to, or is close in value to $E_a(\sigma)$ if the permittivity is independent or shows little temperature dependence. Non ferroelectric materials, 8YSZ and 8D4WSB, have near temperature-independent permittivity and therefore $E_a(f_{max})$ is consistent with $E_a(\sigma)$. Among all the ferroelectric materials investigated in this work, only the Aurivillius phase $Bi_{2.5}Na_{1.5}Nb_3O_{12}$ (m = 3) shows a relatively flat permittivity-temperature profile, Fig.S1 and Fig.5. In this case, $E_a(f_{max})$ is only slightly higher than $E_a(\sigma)$ with a ΔE_a of 3.7%. Furthermore, simulations show that if the phase transition temperature is far outside the measured impedance temperature range, $\log f_{max}$ - T^{-1} will show linear behaviour similar to $\log\sigma$ - T^{-1} plots; however, if T_m is much lower than the lowest temperature investigated, f_{max} will overestimate the activation energy. PZT 5H and $NB_{0.51}T$ represent this case (see Fig.6 and Fig.S9, respectively) and show $E_a(f_{max})$ to be 16.7% and 14.0% higher than $E_a(\sigma)$, respectively. If T_m is much higher than the highest temperature investigated, f_{max} will underestimate the activation energy. Experimentally it is observed in $Bi_{2.5}Na_{0.5}Nb_2O_9$, see Fig.7. If the phase transition occurs within the measurement temperature range, and with a relatively sharp permittivity peak, the $\log f_{max}$ - T^{-1} plot will show an additional (non-linear) feature in the vicinity of T_m. This is observed for PZT 4A, and $Na_{0.5}Bi_{4.5}Ti_4O_{15}$, see Fig.8 and Fig.S11, respectively.

If there is a change in $E_a(\sigma)$ over the temperature range investigated, simulations show that $\log f_{max}$ can still show a linear relationship with T^{-1} given a relatively broad permittivity-temperature profile, which is in agreement with the observation in $NB_{0.49}T$. It should be stressed that as the numerical simulations do not consider the electrical conduction mechanism or type of charge carrier(s), they can be applied to any ferroelectric material. Figs.2 and 3 cover many possible combinations of $\log\sigma - T^{-1}$ and $\varepsilon_r - T$, and can be used to predict the $\log f_{max} - T^{-1}$ relationships for a wide variety of materials.

2) Physical meaning of $E_a(\sigma)$ and $E_a(f_{max})$ in ferroelectric materials

According to Eq.(1), $E_a(\sigma)$ depends only on the temperature dependence and magnitude of the resistance of a material and therefore $E_a(\sigma)$ represents the activation energy for the charge carrier. Depending on the electrical conduction mechanism, it may consist of the migration energy for the charge carrier and the association energy for local defect clusters for ionic conduction,[31] or it may be half of the band gap in the case for an intrinsic semiconductor.[3] Based on Eq.(6), f_{max} is the product of resistance and capacitance, therefore the $\log f_{max} - T^{-1}$ plot contains information from the both conduction and polarisation processes, including their temperature dependence.

Considering a parallel RC circuit, the time constant is defined as the time required to charge the capacitor to 63.2% of the applied voltage through the resistor. For a material with a flat permittivity-temperature profile, the capacitance is constant, so the time constant (and f_{max}) is dependent only on the resistance of the resistor. The temperature dependence of f_{max} is therefore the same as that of σ and therefore $E_a(\sigma)$ and $E_a(f_{max})$ give the same value, as shown by trend-line 1 in Fig.10. For a ferroelectric material below T_m the permittivity increases with increasing temperature and so does the capacitance. It takes a longer time to charge the capacitor with increasing temperature (for an equivalent resistor), and therefore the slope of $\log\tau - T^{-1}$ (or $\log f_{max} - T^{-1}$) deviates from that of $\log\sigma - T^{-1}$ to give a lower $E_a(f_{max})$ than $E_a(\sigma)$, as illustrated by trend-line 2 in Fig.10. Above T_m, the permittivity and consequently the capacitance decreases with increasing temperature. Therefore, it takes shorter time to charge the capacitor with increasing temperature and results in a larger slope on the $\log f_{max} - T^{-1}$ plot, so $E_a(f_{max})$ is higher than $E_a(\sigma)$ in this region. $E_a(f_{max})$ is therefore an indication of how the polarisation or orientation of the dipoles present in the material interact with the charge carriers. The larger the difference between $E_a(f_{max})$ and $E_a(\sigma)$, the bigger is the influence from the lattice polarisation.

Published on 13 August 2018. Downloaded by University of Sheffield on 8/14/2018 9:16:36 AM.

Journal of Materials Chemistry C Accepted Manuscript

Please do not adjust margins

View Article Online
DOI: 10.1039/C8TC03011A

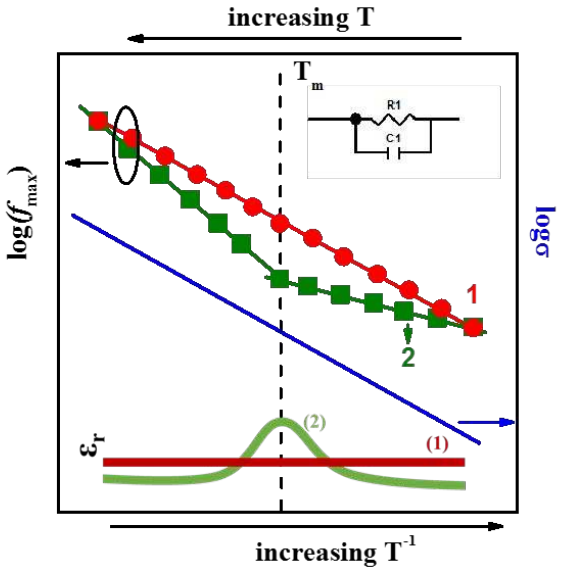

Fig.10 Schematic of the change of logf_{max} – T^{-1} relationship for a parallel RC circuit when the capacitor shows different dependences on temperature: (1) capacitance does not change with temperature and (2) capacitance changes with temperature with a maximum at T_m. Inset figure at the bottom shows the corresponding ε_r – T relationship.

Concluding remarks

In this paper, we study the $E_a(\sigma)$ and $E_a(f_{max})$ for some typical non-ferroelectric and ferroelectric materials and employ numerical simulations to investigate combinations of different logσ –T^{-1} and ε_r – T profiles on the logf_{max} – T^{-1} relationship and $E_a(f_{max})$. Both experimental and simulation results show both the ε_r – T profile and the temperature range relative to T_m are critical to the logf_{max} – T^{-1} relationship and $E_a(f_{max})$ values. Major conclusions are:

1) Non-ferroelectric materials with temperature-independent (or nearly temperature-independent) permittivity or ferroelectric/relaxor materials with relatively flat permittivity-temperature profiles, $E_a(\sigma)$ and $E_a(f_{max})$ are identical or very similar. In such cases, $E_a(f_{max})$ can be used to estimate $E_a(\sigma)$.
2) For ferroelectric materials with a sharp permittivity peak at T_m, the logf_{max} – T^{-1} plot can show non-linear behaviour. $E_a(f_{max})$ is dependent on the temperature range measured relative to T_m. If the temperature range studied is much higher than T_m, $E_a(f_{max})$ is larger than $E_a(\sigma)$; if it is much lower than T_m, then $E_a(f_{max})$ is lower than $E_a(\sigma)$. If T_m is within the temperature range studied, logf_{max} – T^{-1} can deviate from a linear relationship and therefore it is not possible to reliably calculate $E_a(f_{max})$. Any values obtained for $E_a(f_{max})$ will have significant errors associated with them and such analysis is not recommended.
3) The simulation results in Figs.2 and 3 can be applied to many ferroelectric and related materials with different logσ –T^{-1} and ε_r – T profiles and show the use of $E_a(f_{max})$ to obtain the activation energy for bulk electrical conduction (and any discuss of the possible conduction mechanisms) in ferroelectric materials should be used with caution.
4) Here we have focused on presenting impedance data in the form of Z* and M''-log$f$ spectroscopic plots. Other formalisms and plots of impedance data, i.e., M'-log$f$, Z''-log$f$, C' – log$f$, Y'-log$f$, tanδ-log$f$, etc., can also provide valuable information on the dynamics of these materials and are worthy of further study.

Conflict of interest

There are no conflicts to declare.

Acknowledgements

We thank the EPSRC for funding EP/L027348/1. E. Pradal-Velázquez thanks CONACYT for his scholarship under "Becas CONACYT al extranjero (registro 327115)".

References

1 J. F. Scott, Science, 2007, 315, 954.
2 L. W. Martin and A. M. Rappe, Nat. Rev. Mater., 2016, 2, 16087.
3 M. Li, M. J. Pietrowski, R. A. De Souza, H. Zhang, I. M. Reaney, S. N. Cook, J. A. Kilner and D. C. Sinclair, Nat. Mater., 2014, 13, 31.
4 M. Li, H. Zhang, S. N. Cook, L. Li, J. A. Kilner, I. M. Reaney and D. C. Sinclair, Chem. Mater., 2015, 27, 629.
5 L. Li, M. Li, H. Zhang, I. R. Reaney and D. C. Sinclair, J. Mater. Chem. C, 2016, 4, 5779.
6 F. Yang, M. Li, L. Li, P. Wu, E. Pradal-Velázquez and D. C. Sinclair, J. Mater. Chem. A, 2018, 6, 5243.
7 J. T. S. Irvine, D. C. Sinclair and A. R. West, Adv..Mater., 1990, 2, 132.
8 M. J. Verkerk, B. J. Middelhuis and A. J. Burggraaf, Solid State Ionics, 1984, 6, 159.
9 J. R. Macdonald, Impedance spectroscopy- Emphasizing solid materials and systems, Wiley, New York, USA, 1987.
10 F. Yang, X. Zhao and P. Xiao, J. Power Sources, 2011, 196, 4943.
11 S. Saha and T. P. Sinha, J. Appl. Phys., 2006, 99, 014109.
12 A. Molak, M. Paluch, S. Pawlus, J. Klimontko, Z. Ujma and I. Gruszka, J. Phys. D: Appl. Phys., 2005, 38, 1450.
13 Ak. Anirban, T. Paul, Proloy T. Das, T. K. Nath and A. Dutta, Solid State Ionics, 2015, 270, 73.
14 J. Hou, R. Vaish, Y. Qu, D. Krsmanovic, K. B. R. Varma and R. V. Kumar, J. Power Sources, 2010, 195, 2613.
15 Z. G. Yi, Y. X. Li, Y. Wang and Q. R. Yin, J. Electrochem. Soc., 2006, 153, F100.
16 A. Karmakar, S. Majumdar and S. Gin, Phys. Rev. B, 2009, 79, 094406.
17 P. K. Panda and B. Sahoo, Ferroelectrics, 2015, 474, 128.
18 N. Horchidan, C. E. Ciomaga, R. C. Frunza, C. Capiani, C. Galassi and L. Mitoseriu, Ceram. Int., 2016, 42, 9125.
19 I. W. Chen, J. Phys. Chem. Solids, 2000, 61, 197.
20 K. R. Kendall, C. Navas, J. K. Thomas and H. zur Loye, Chem. Mater., 1996, 8, 642.
21 A. D. Rae, J. G. Thompson, R. L. Whithers and A. C. Willis, Acta Crystallogr. B, 1990, 46, 474.
22 C. H. Hervoches, A. Snedden, R. Riggs, S. H. Kilcoyne, P. Manuel and P. Lightfoot, J. Solid State Chem., 2002, 164, 280.
23 A. Moure, Appl. Sci., 2018, 8, 62.
24 J. G. fletcher, A. R. West and J. T. S. Irvine, J. Electrochem. Soc., 1995, 142, 2650.
25 S. T. Amaral and I. L. Muller, Corrosion, 1999, 55, 17.

Published on 13 August 2018. Downloaded by University of Sheffield on 8/14/2018 9:16:36 AM.

Journal of Materials Chemistry C Accepted Manuscript

This journal is © The Royal Society of Chemistry 20xx

Please do not adjust margins

Journal Name ARTICLE

View Article Online
DOI: 10.1039/C8TC03011A

26 J. Fleig, Solid State Ionics, 2002, 150, 181.
27 X. Guo and R. Waser, Prog. Mater. Sci., 2006, 51, 151.
28 F. Yang, H. Zhang, L. Li, I. M. Reaney and D. C. Sinclair, Chem. Mater., 2016, 28, 5269.
29 L. Koch, S. Steiner, K. C. Meyer, I. T. Seo, K. Albe and T. Fromling, J. Mater. Chem. C, 2017, 5, 8958.
30 D. W. Jung, K. L. Duncan and E. D. Wachsman, Acta Mater., 2010, 58, 355.
31 D. J. Kim, J. Am. Ceram. Soc., 1989, 72, 1415.

Published on 13 August 2018. Downloaded by University of Sheffield on 8/14/2018 9:16:36 AM.

Journal of Materials Chemistry C Accepted Manuscript

Please do not adjust margins

View Article Online
DOI: 10.1039/C8TC03011A

Table of contents

- The use of time constant related parameter f_{max} *to* obtain the activation energy for bulk electrical conduction (and any discuss of the possible conduction mechanisms) in ferroelectric materials should be used with caution.

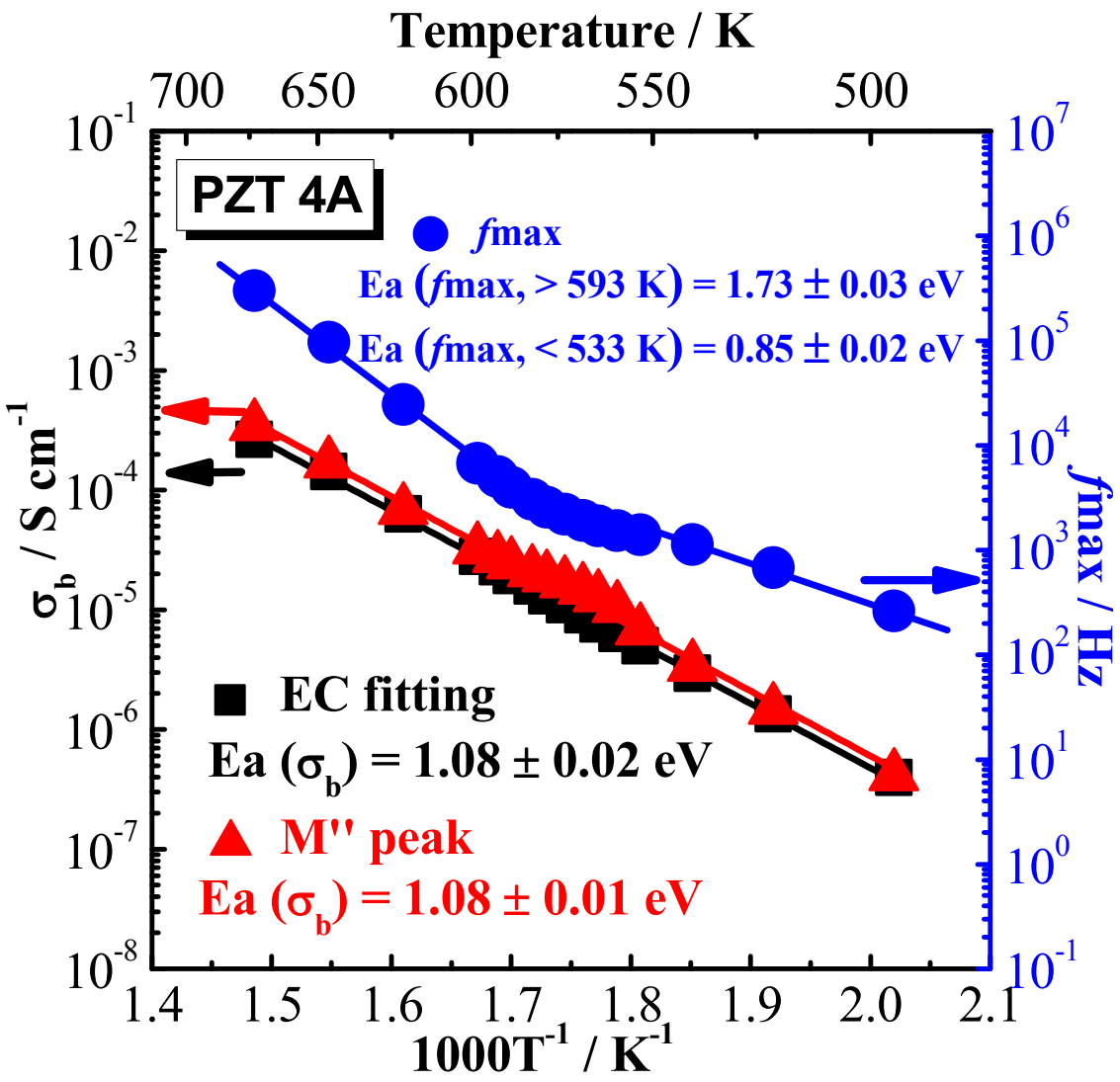

Published on 13 August 2018. Downloaded by University of Sheffield on 8/14/2018 9:16:36 AM.

Journal of Materials Chemistry C Accepted Manuscript